

**Figure S1. Loss of *Mll4* induces enhanced IFN- $\gamma$  expression in Th1 cells, related to Figure 1.**

(A) ELISA assessment of IFN- $\gamma$  in the culture medium in WT and *Mll4* KO cells under either naïve state or Th1 condition (24 h).

(B) qPCR analysis of mRNAs in WT and *Mll4* KO CD4<sup>+</sup> T cells under either naïve state or Th1 condition (24 h); results are presented relative to those of *Gapdh*.

(C) Immunoblot analysis of p-STAT4, STAT4 and total H3 in WT and *Mll4* KO Th1 cells.

(D) Volcano plots of differentially expressed genes (DEGs) from RNA-seq data in WT and *Mll4* KO naïve CD4<sup>+</sup> T cells and Th1 cells. Fold changes (KO/WT) and P-values were reported by Cuffdiff. Fold change > 2 (or < 0.5) and P-value smaller than 0.001 were set as the significant cutoffs. The RNA-seq data were generated in this study.

(E) Enriched GO terms for up-regulated DEGs in *Mll4* KO cells. Only top five terms were shown. Data are representative of at least two independent experiments (A-C). \*\*\*p < 0.001. (Student's *t*-test, error bars represent SD).

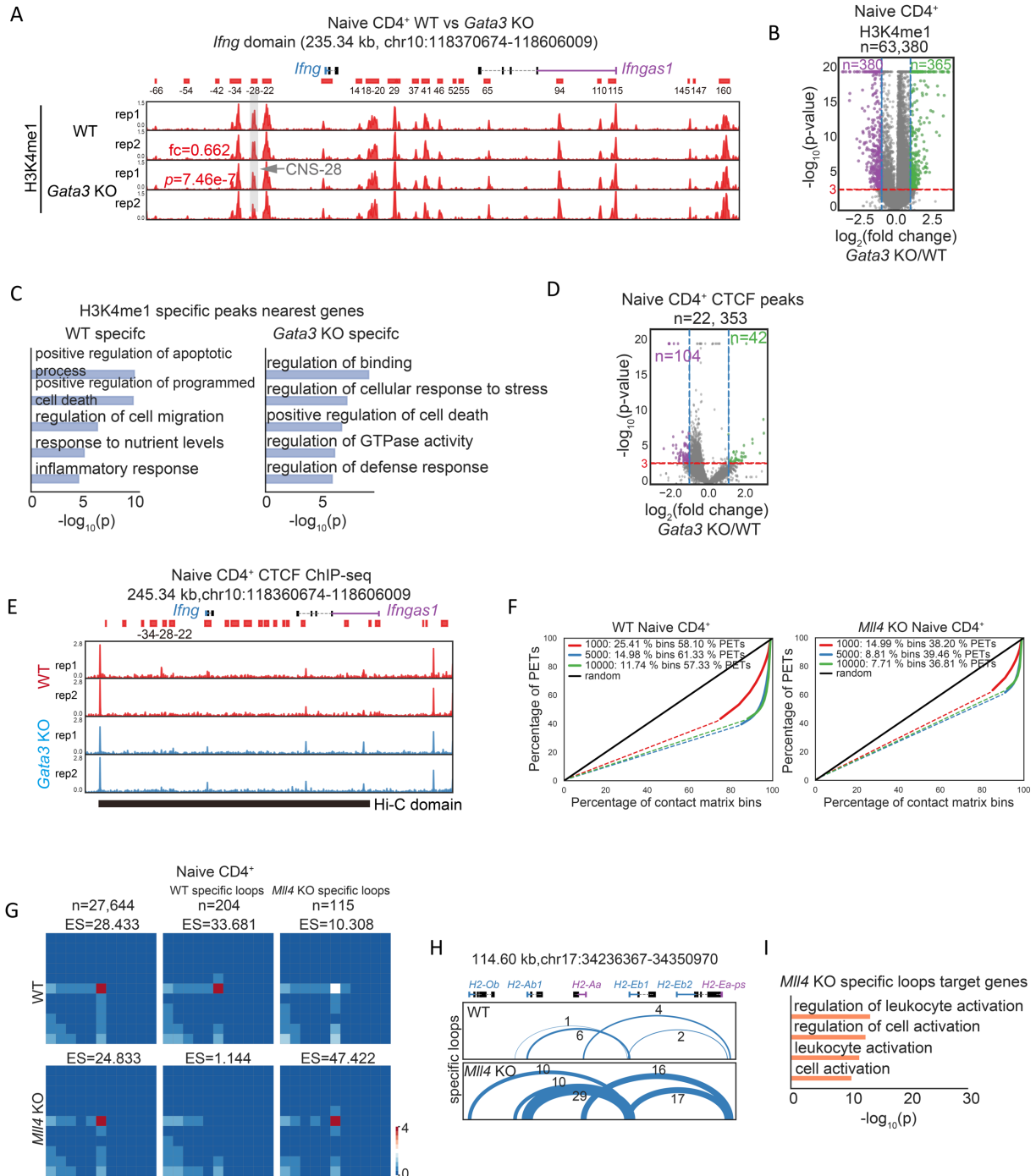


**Figure S2. GATA3 acts downstream of MLL4 on CNS-28, related to Figure 2.**

(A) Genome browser images of H3K4me1 ChIP-seq profiles at the *lfng* locus in naïve CD4<sup>+</sup> T cells isolated from WT and *Gata3* KO mice. The ChIP-seq data were generated in this study. Fold change (KO/WT) and Poisson test *p*-value at the CNS-28 locus were shown for average normalized reads from two replicates by comparing WT and *Gata3* KO data.

(B) Volcano plots of significantly changed H3K4me1 peaks. Mean values from two replicates were used to calculate fold changes (KO/WT) and Poisson *P*-values. Fold change > 2 (or < 0.5) and *P*-value smaller than 0.001 were set as the significant cutoffs. Numbers of total peaks, WT specific peaks and KO specific peaks are shown.

(C) Enriched GO terms for the closest genes associated with significantly changed H3K4me1 peaks (B). Only top five terms were shown.

(D) Volcano plots of significantly changed CTCF peaks for naïve CD4<sup>+</sup> T cells from WT and *Gata3* KO mice. Mean values from three replicates were used to calculate fold changes (KO/WT) and Poisson *P*-values. Fold change > 2 (or < 0.5) and *P*-value smaller than 0.001 were set as the significant cutoffs. Numbers of total peaks, WT specific peaks and KO specific peaks were shown.

(E) CTCF ChIP-seq Genome Browser tracks for the *Ifng* locus in WT and *Gata3* KO naïve CD4<sup>+</sup> T cells were shown. The CTCF ChIP-seq data were generated in this study.

(F) Analysis of the interaction resolution for pooled Hi-TrAC data. The analysis was performed similarly with the previous studies.<sup>1,2</sup> Briefly, in one colorful curve, the dashed line shows the bins from the contact matrix with only singleton PET, and the solid lines show the bins with multiple PETs for one specific resolution. The solid black line indicates all PETs are evenly distributed in the contact matrix bins. The highest estimated interaction resolution is defined as more than 50% non-singleton PETs in the defined bin sizes (as here for 1kb bin size).

(G) Analysis of differentially enriched chromatin loops in WT and *Mll4* KO naïve CD4<sup>+</sup> T cells from Hi-TrAC data. The analysis was performed by the cLoops2 callDiffLoops module with default parameters. A total of 27,963 loops were called from pooled naïve CD4<sup>+</sup> T cell Hi-TrAC data, requiring at least 20 PETs supporting a loop. WT and *Mll4* KO Hi-TrAC libraries were down-sampled to 35 million high-quality unique PETs for the analysis.

(H) An example of a genomic region with stronger chromatin loops in *Mll4* deletion cells. Only *Mll4* KO-specific loops and numbers of PETs detected for each loop were shown in the comparison.

(I) Enriched GO terms for genes associated with stronger chromatin loops in *Mll4* deletion cells. No enriched GO terms were found for wild-type specific loops.

Data are representative of at least two independent experiments (A-I).

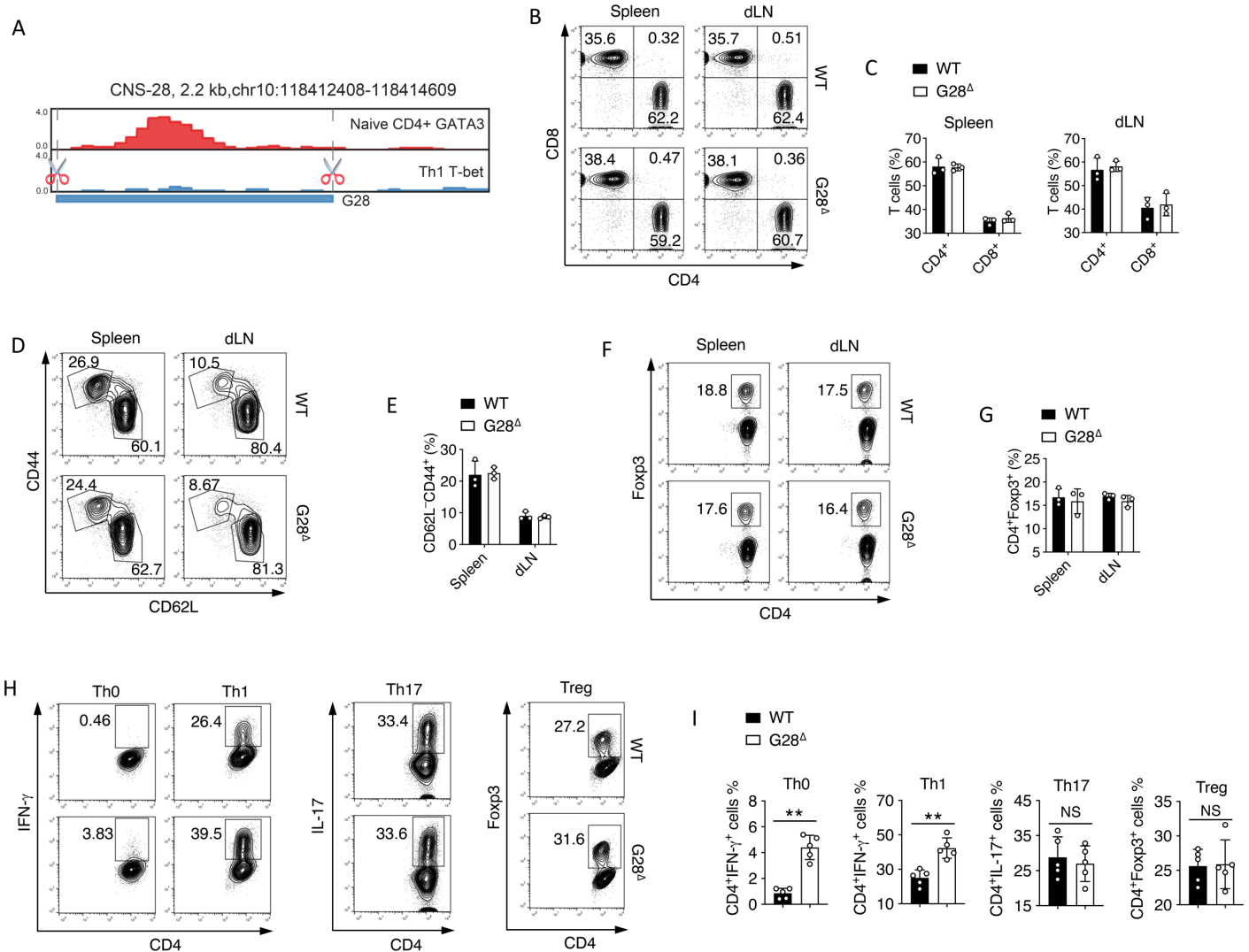


**Figure S3. CNS-28 suppresses IFN- $\gamma$  expression, related to Figure 3.**

(A) Generation of G28<sup>Δ</sup> mice by deleting a genomic region of about 1kb around the GATA-3 binding site by CRISPR (scissors).

(B-C) (B) Flow cytometry analysis and (C) quantification of CD4 and CD8 expression on CD45<sup>+</sup> cells from spleen and peripheral lymph nodes (dLN) of WT and G28<sup>Δ</sup> mice at 8 weeks of age.

(D-E) (D) Flow cytometry analysis and (E) quantification of CD44 and CD62L expression on CD4<sup>+</sup> T cells from spleen and peripheral lymph nodes (dLN) of WT and G28<sup>Δ</sup> mice at 8 weeks of age.

(F-G) (F) Flow cytometry analysis and (G) quantification of Foxp3 expression on CD4<sup>+</sup> T cells from spleen and peripheral lymph nodes (dLN) of WT and G28<sup>Δ</sup> mice at 8 weeks of age.

(H-I) Naive CD4<sup>+</sup> T cells from WT and G28<sup>Δ</sup> mice were stimulated under Th0, Th1, Th17 and pTreg conditions and harvested at 72 hours. Intracellular staining of indicated cytokines produced

by different polarized T cell subsets cells from WT and G28<sup>Δ</sup> mice was determined by (H) flow cytometry and (I) Quantification.

Data are representative of at least two independent experiments (B-I). \*\*p < 0.01. NS: not statistically significant. (Student's *t*-test, error bars represent SD).

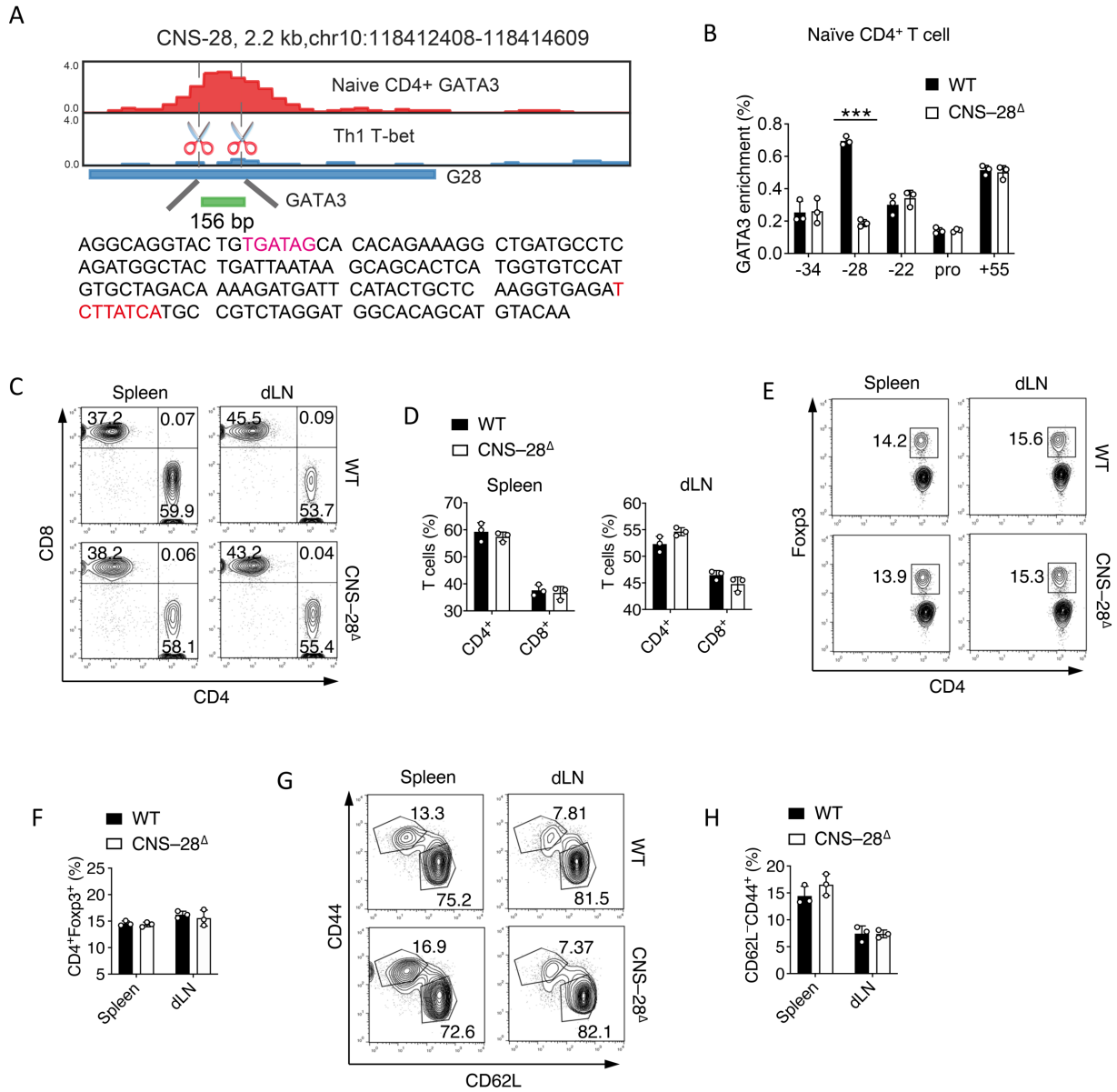


**Figure S4. CNS-28 is critical for systemic immune homeostasis, related to Figure 3.**

(A) Generation of CNS-28<sup>Δ</sup> mice by deleting a genomic region of 156bp containing two GATA-3 motifs by CRISPR (scissors).

(B) ChIP-qPCR analysis of GATA-3 binding to the *Ifng* locus in WT or CNS-28<sup>Δ</sup> naïve CD4<sup>+</sup> T cells, presented relative to input.

(C-D) (C) Flow cytometry analysis and (D) quantification of CD4 and CD8 expression on CD45<sup>+</sup> cells from spleen and peripheral lymph nodes (dLN) of WT and CNS-28<sup>Δ</sup> mice at 8 weeks of age.

(E-F) (E) Flow cytometry analysis and (F) quantification of Foxp3 expression on CD4<sup>+</sup> T cells from spleen and peripheral lymph nodes (dLN) of WT and CNS-28<sup>Δ</sup> mice at 8 weeks of age.

(G-H) (G) Flow cytometry analysis and (H) quantification of CD44 and CD62L expression on CD4<sup>+</sup> T cells from spleen and peripheral lymph nodes (dLN) of WT and CNS-28<sup>Δ</sup> mice at 8 weeks of age.

Data are representative of three independent experiments (B-H). \*\* $p < 0.01$ . NS: not statistically significant. (Student's *t*-test, error bars represent SD).

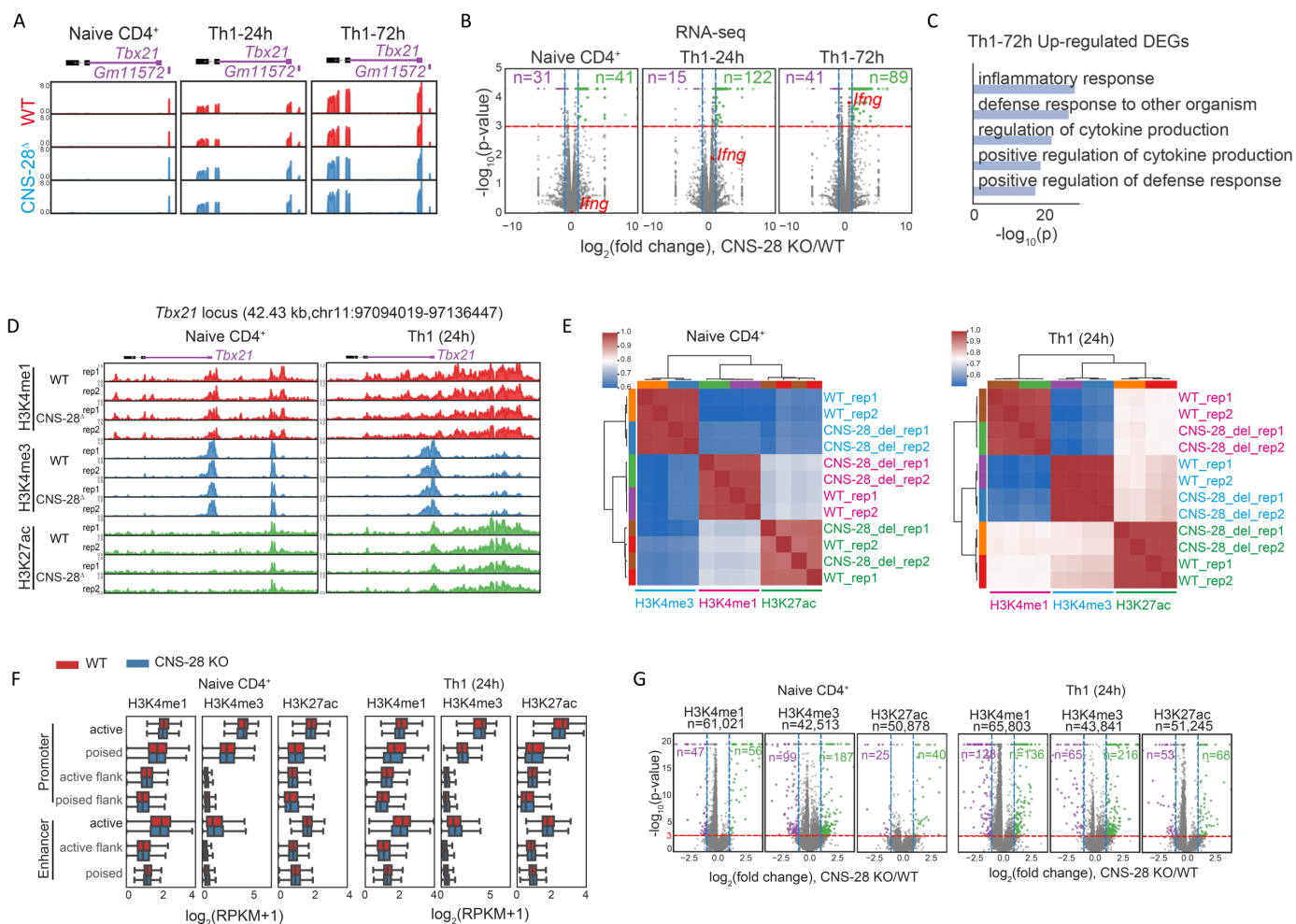


**Figure S5. The effect of CNS-28 is mainly limited to the *Ifng* locus, related to Figure 4.**

(A) Genome browser images of *Tbx21* expression levels from RNA-seq data during Th1 differentiation comparing WT and CNS-28<sup>Δ</sup> T cells.

(B) Volcano plots of differentially expressed genes between WT and CNS-28<sup>Δ</sup> cells under naïve state and Th1 conditions. Fold changes (KO/WT) and *P*-values were reported by Cuffdiff. Fold change > 2 (or < 0.5) and *P*-value smaller than 0.001 were set as the significant cutoffs. The RNA-seq data were generated in this study.

(C) Enriched GO terms for up-regulated differentially expressed genes in CNS-28<sup>Δ</sup> Th1 cells (72 hr). Only top five terms were shown.

(D) Genome browser images of H3K4me1, H3K4me3 and H3K27ac ChIP-seq profiles in the *Tbx21* domain in WT and CNS-28<sup>Δ</sup> naïve CD4<sup>+</sup> T and Th1 cells. The ChIP-seq data were generated in this study.

(E) Sample-wise genome-wide similarity analysis for ChIP-seq comparing WT and CNS-28<sup>Δ</sup> naïve CD4<sup>+</sup> T cells and Th1 cells.

(F) Distribution of ChIP-seq signals at different genomic segments in naïve CD4<sup>+</sup> T cells and Th1 cells. Genomic segments were defined from overlaps of H3K4me1, H3K4me3 and H3K27ac ChIP-seq peaks described previously.<sup>3</sup>

(G) Volcano plots of significantly changed histone modification peaks in CNS-28<sup>Δ</sup> naïve CD4<sup>+</sup> T cells and Th1 cells. Mean values from two replicates were used to calculate fold changes (KO/WT) and Poisson *p*-values. Fold change > 2 (or < 0.5) and *p*-value smaller than 0.001 were set as the significant cutoffs. Numbers of total peaks, WT and KO specific peaks are shown.

Data are representative of at least two independent experiments (A-G).

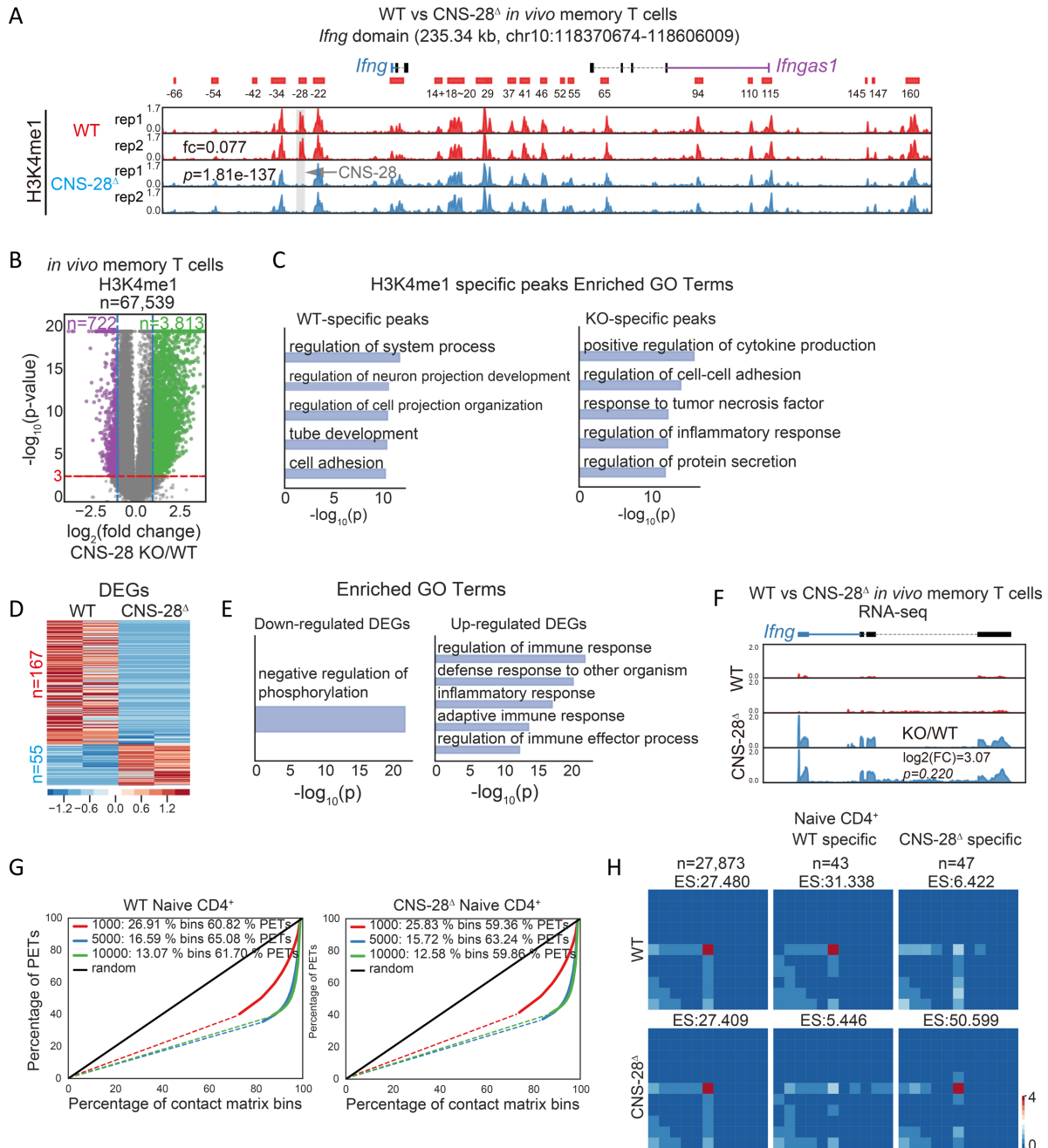


**Figure S6. CNS-28 suppresses *Ifng* expression in memory CD4<sup>+</sup> T cells, related to Figure 4.**

(A) Genome browser images of H3K4me1 ChIP-seq signals for the *Ifng* domain in the memory CD4<sup>+</sup> T cells isolated from WT and CNS-28<sup>Δ</sup> mice. The ChIP-seq data were generated in this study. Fold change and Poisson test *p*-value were shown for normalized reads at CNS-28 locus for comparing WT and CNS-28<sup>Δ</sup> cells.

(B) Volcano plots of significantly changed histone modification peaks in WT and CNS–28<sup>Δ</sup> memory CD4<sup>+</sup> T cells. Peaks were called by the cLoops2 callPeaks module and compiled as a union set for the same histone modification. Mean values from two replicates were used to calculate fold changes (KO/WT) and Poisson *p*-values. Fold change > 2 (or < 0.5) and *p*-value smaller than 0.001 were set as the significant cutoffs. Numbers of total peaks, WT and KO specific peaks were shown.

(C) Enriched GO terms for the closest genes associated with significantly changed H3K4me1 peaks. Only top five terms were shown.

(D) Heatmap of differentially expressed genes comparing WT and CNS–28<sup>Δ</sup> memory CD4<sup>+</sup> T cells.

(E) Enriched GO terms for differentially expressed genes affected by CNS–28 deficiency. Only top five terms were shown for up-regulated genes and only one term was found significant for down-regulated genes.

(F) Genome browser images of *Ifng* expression from RNA-seq data in WT and CNS–28<sup>Δ</sup> memory CD4<sup>+</sup> T cells. Fold change (KO/WT) and *p*-value for *Ifng* were reported by Cuffdiff.

(G) Analysis of interaction resolution for pooled Hi-TrAC data generated using WT and CNS–28<sup>Δ</sup> naïve CD4<sup>+</sup> T cells. The analysis was performed similarly with the previous studies.<sup>1,2</sup> Briefly, in one colorful curve, the dashed line shows the bins from the contact matrix with only singleton PET, and the solid lines show the bins with multiple PETs for one specific resolution. The solid black line indicates all PETs are evenly distributed in the contact matrix bins. The highest estimated interaction resolution is defined as more than 50% non-singleton PETs in the defined bin sizes (as here for 1kb bin size).

(H) Analysis of differentially enriched loops using Hi-TrAC data from WT and CNS–28<sup>Δ</sup> naïve CD4<sup>+</sup> T cells. WT and CNS–28<sup>Δ</sup> Hi-TrAC libraries were down-sampled to 37 million high-quality unique PETs for the analysis.

Data are representative of two independent experiments (A-H).

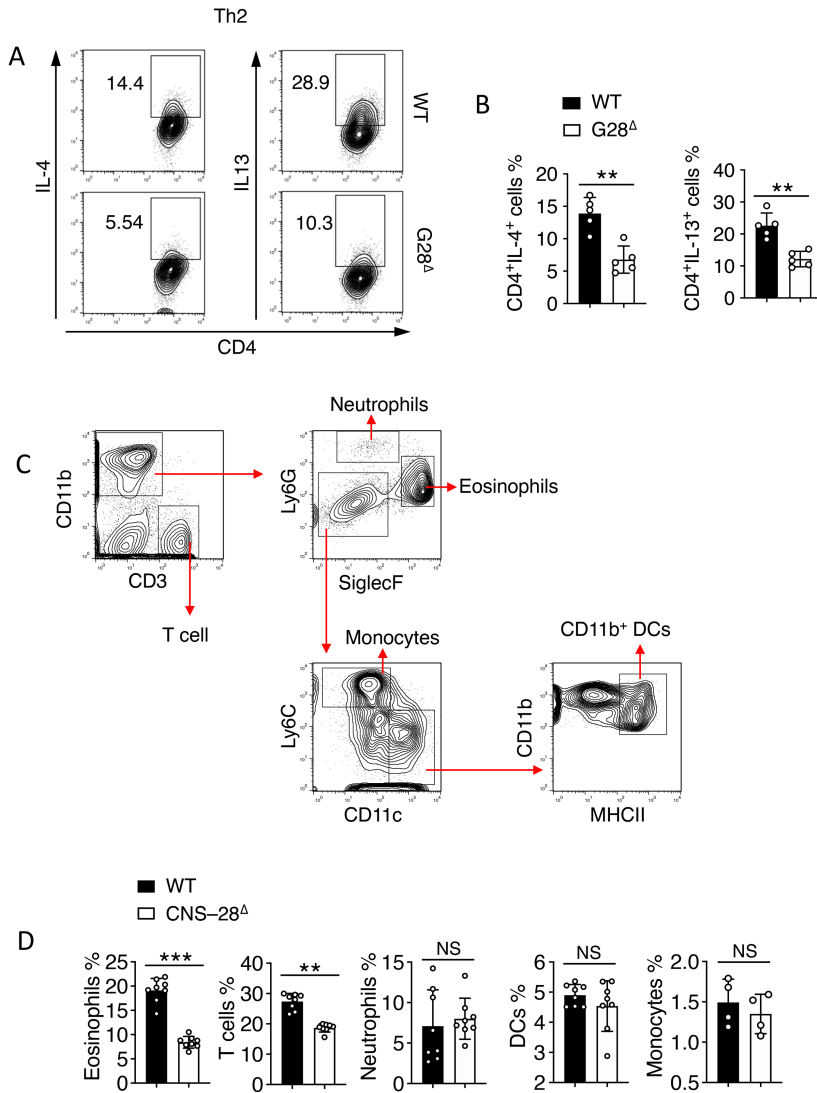


**Figure S7. CNS–28 is critical for type 1 responses during host defense and inflammation, related to Figure 6.**

(A-B) Naive CD4<sup>+</sup> T cells from WT and G28<sup>Δ</sup> mice were stimulated under Th2 condition and harvested at 72 hours. Intracellular staining of indicated cytokines was determined by (A) flow cytometry and (B) Quantification.

(C) Gating strategy for eosinophils, T cells, neutrophils, DCs and monocytes isolated from lung 10 days after HDM induction.

(D) Quantification of inflammatory cells percentage in the lung tissue of WT and CNS–28<sup>Δ</sup> mice, assessed at 10 days after HDM challenge.

Data are representative of three independent experiments (A, B, D). \*\*p < 0.01, \*\*\*p < 0.001 (Student's t test, error bars represent SD).

**Reference:**

1. Liu, S., Cao, Y., Cui, K., Tang, Q., and Zhao, K. (2022). Hi-TrAC reveals division of labor of transcription factors in organizing chromatin loops. *Nat Commun* 13, 6679. 10.1038/s41467-022-34276-8.
2. Cao, Y., Liu, S., Ren, G., Tang, Q., and Zhao, K. (2022). cLoops2: a full-stack comprehensive analytical tool for chromatin interactions. *Nucleic Acids Res* 50, 57-71. 10.1093/nar/gkab1233.
3. Cao, Y., Liu, S., Cui, K., Tang, Q., and Zhao, K. (2022). Hi-TrAC reveals fractal nesting of super-enhancers. *bioRxiv*, 2022.2007.2013.499926. 10.1101/2022.07.13.499926.